ACS APPLIED MATERIALS & INTERFACES

www.acsami.org Research Article

Ultrathin Atomic Layer Deposited Al_2O_3 Overcoat Stabilizes Al_2O_3-Pt/Ni-Foam Hydrogenation Catalysts

Azina Rahmani, Maksim A. Sultanov, Kemah Kamiru-White, Lorianne R. Shultz-Johnson, Brian E. Butkus, Shaohua Xie, Fudong Liu, Diep T. H. Nguyen, Noémie Wilson-Faubert, Ali Nazemi, Parag Banerjee, Lei Zhai, Massimiliano Delferro, Jianguo Wen,* and Titel Jurca*

Cite This: *ACS Appl. Mater. Interfaces* 2023, 15, 43756−43766 Read Online

ABSTRACT: Galvanic exchange seeds the growth of Pt nanostructures on the Ni foam monolith. Subsequent atomic layer deposition of ultrathin Al_2O_3 followed by annealing under air affords supported Pt catalysts with ultralow loading (0.020 ppm). In addition to the expected enhancement of the stability of the Pt particles on the surface, the ∼2 nm Al_2O_3 overcoat appears to also play a crucial role in the overall structural integrity of the NiO_x nanoplates that grow on the Ni foam surface as a result of the preparative route. The resulting material is physically robust toward repeated handling and showcases retention of catalytic activity over 10 standard catalyst recycling trials, standing in marked contrast to the uncoated samples. Catalyst activity was tested via the hydrogenation of various functionalized styrenes at low temperatures and low hydrogen pressure in ethanol as a solvent, with a TOF as high as 9.5×10^6 h^{-1} for unfunctionalized styrene. Notably, the catalysts show excellent tolerance toward F, Cl, and Br substituents and no hydrogenation of the aromatic ring.

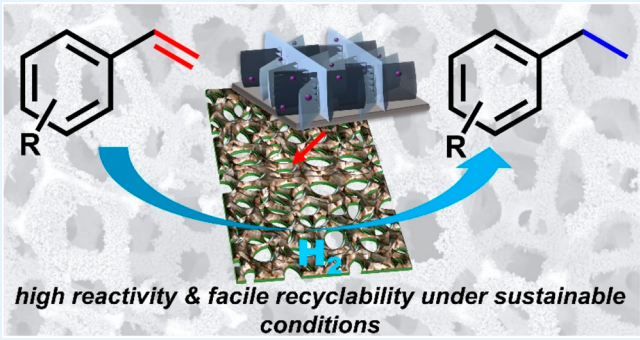

KEYWORDS: *heterogeneous catalysis, hydrogenation, nickel foam, atomic layer deposition, platinum catalyst*

INTRODUCTION

Heterogeneous catalysts based on platinum enable a vast array of important thermocatalytic and electrocatalytic chemical transformations in the service of both commodity and fine chemical synthesis. These include but are not limited to methylation of amines,[1] olefin isomerization,[2] olefin epoxidation,[3] alcohol oxidation,[4] hydrosilylations,[5] and germane to this report, hydrogenation of nitro,[6,7] alkene,[8−11] and alkyne groups.[12,13] When paired with its relatively low natural abundance, limited options for supply,[14] and broad demand, Pt becomes a high priced commodity. To offset the cost and ensure long-term availability while benefiting from its high reactivity under typically mild reaction conditions, Pt-based catalyst systems must be designed to minimize the amount of Pt and maximize recovery and reusability.

One of our groups has recently demonstrated a hierarchical Pd on nickel foam hydrogenation catalyst system that requires very low Pd loadings and is readily recoverable and reusable.[15] Herein, this general strategy is exploited for the development of Ni foam-supported Pt catalysts. Ni foam monolith supports offer a number of advantages over more conventional systems such as carbonaceous or metal oxide powders, for example, ease of handling and separability afforded by the contiguous framework,[16] a porous three-dimensional (3-D) membrane framework (Figures 1 and 2a) amenable to application in continuous flow catalysis,[15,17] the potential for resistive heating,[18] and ferromagnetism which enables self-stirring, eliminating trace impurities on stir bars as a contamination vector.[19] Ni foam-supported Pt catalysts have previously been reported for electrocatalysis applications.[20−26] To the best of our knowledge, these types of catalyst systems have not been utilized or optimized for thermocatalytic hydrogenation

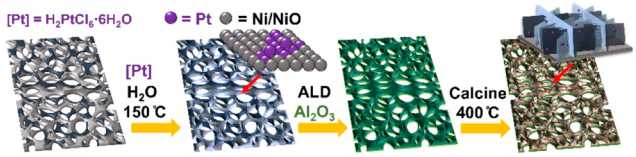

Figure 1. Schematic representation for the galvanic displacement of Ni with Pt, growth of clustered/sheet-like Pt, subsequent ALD Al_2O_3 overcoating, and calcination under air to produce **Al_2O_3-Pt/Ni**.

Received: June 19, 2023
Accepted: August 28, 2023
Published: September 11, 2023

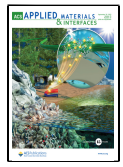

https://doi.org/10.1021/acsami.3c08545
ACS Appl. Mater. Interfaces 2023, 15, 43756−43766

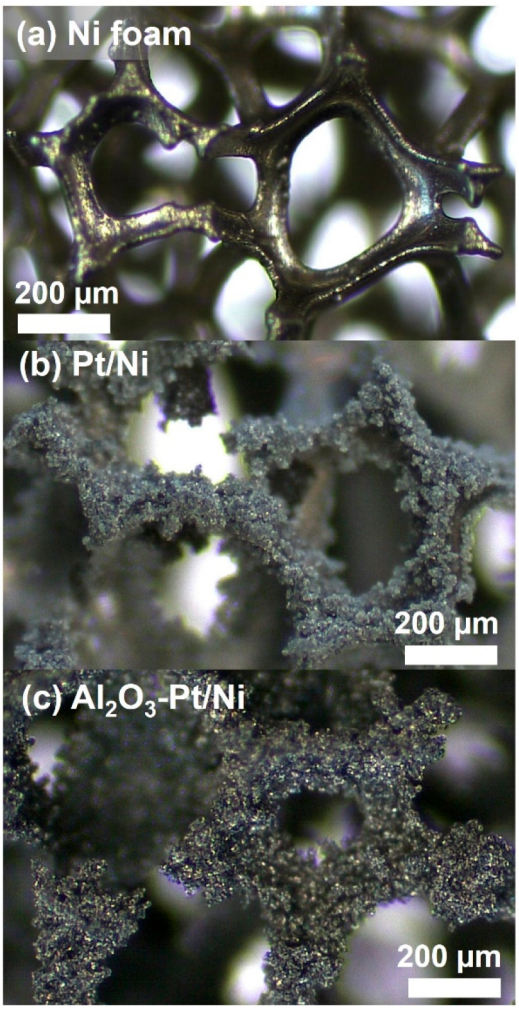

Figure 2. Optical micrographs of Ni foam (a), **Pt/Ni** (b), and **Al_2O_3-Pt/Ni** (c).

reactions, a critical subset of reactions with broad applications in both petrochemical and fine chemical industries.[27]

In this report, the preparation of Ni foam-supported Pt catalysts created first through a conventional galvanic exchange process with a Pt precursor, followed by atomic layer deposition (ALD) of an ultrathin (~2 nm) Al_2O_3 encapsulant, with subsequent calcination is reported. The process yields Ni foams covered with Al_2O_3-coated NiO (with partial Ni_2O_3 domains) nano-to-microplates and very sparse, ultralow loading of Pt (Figure 1). The resulting catalysts display remarkable reactivity for the hydrogenation of styrene and its derivatives, with complete tolerance toward halide substituents, all under very mild and sustainable reaction conditions (low temperature, low H_2 pressure, and ethanol as solvent). ALD Al_2O_3 has been explored broadly in support of catalyst overcoating.[28−32] The resulting process typically yields enhanced performance, citing a reduction of sintering and leaching due to physical blocking of metal nanoparticle mobility and the potential to modify selectivity by preferential ALD Al_2O_3 growth on undercoordinated nanoparticle sites, leaving terrace sites uncoated. In preparing complementary materials without ALD Al_2O_3 overcoat, dramatically enhanced stability and long-term performance are observed for the ALD overcoated samples, not only for the Pt-promoted catalysis but also for the physical integrity of the NiO_x surface nanostructures on which the Pt is supported.

■ EXPERIMENTAL SECTION

Chemicals and Materials. Nickel foam was purchased from MTI Corporation as 1.6 mm thick roll (1000 mm × 300 mm), with >99.9 wt % Ni purity. $H_2PtCl_6{\cdot}6H_2O$ was purchased from Acros Organics. Ultrahigh purity H_2 and argon gas were supplied by Airgas. Absolute ethanol, toluene, and hydrochloric acid were purchased from Fisher Chemical. 4-Nitrostyrene, 4-vinylphenol (stabilized with propylene glycol), 2,4,6-trimethylstyrene, 4-methylstyrene, 4-bromostyrene, 4-chlorophenylacetylene, 4-methoxystyrene, and $CDCl_3$ were purchased from Alfa Aesar. 4-Chlorostyrene, 4-(trifluoromethyl)styrene, and 1-ethynyl-4-fluorobenzene were purchased from Tokyo Chemical Industry (TCI). Styrene and trimethylaluminum (TMA), with ≥97% purity, were purchased from Sigma-Aldrich. Phenylacetylene was purchased from Thermo Scientific Chemicals. Water used in all of the experiments was deionized (DI) water. All chemicals were used as received under an ambient lab atmosphere without further purification, except TMA, which requires handling under inert atmosphere.

Materials Synthesis. Ni foam was cut into square blocks and then subjected to ultrasonic cleaning in concentrated hydrochloric acid solution (0.15 M) for 5 min at room temperature. Subsequently, the foams were rinsed with DI water and dried in an oven at 150 °C overnight. To induce the deposition of Pt on the Ni foam, cleaned foams (~4 g) were immersed in an aqueous solution of platinum precursor (500 mg of $H_2PtCl_6{\cdot}6H_2O$ dissolved in 200 mL of DI water) at 150 °C under stirring in a sealed 400 mL heavy wall high pressure flask. After 21 h, the foams were removed from the reaction flask and rinsed with DI water. The functionalized Ni foams were then dried in an oven at 150 °C overnight. Afterwards, half of the materials were transferred to a quartz container, placed in a furnace, and annealed under lab atmosphere at 400 °C for 1 h at a heating rate of 5 $°C{\cdot}min^{-1}$. The resulting sample is labeled **Pt/Ni**. The remaining foams were treated with a thin Al_2O_3 overcoat via a thermal atomic layer deposition (ALD) process. ALD of Al_2O_3 was performed in a Fiji Gen2 ALD system from Veeco at 120 °C. The precursors for deposition are TMA and DI water purified by a Direct-Q Millipore system. The recipe for one Al_2O_3 cycle consisted of a 60 ms pulse of TMA and a 60 ms pulse of DI water. The reaction chamber was purged between each pulse with a 10 s flow of argon at 75 standard cubic centimeters per minute (sccm). One standard recipe was used, but cycles varied based on in situ spectroscopic ellipsometry data. One batch of nickel foam was subjected to 30 cycles of Al_2O_3 which corresponds to a thickness of 2.17 nm on a planar silicon substrate. To measure the thickness of the Al_2O_3 overlayer, silicon coupons were run during the process and measured in situ using ellipsometry: J.A. Woollam M2000 spectroscopic ellipsometer with a wavelength range from 280 to 1690 nm. All optical models for thin-film analysis were built in J.A. Woollam's Complete Ease software. Lastly, the samples were similarly annealed under a lab atmosphere at 400 °C for 1 h at a heating rate of 5 $°C{\cdot}min^{-1}$. The resulting material is labeled **Al_2O_3-Pt/Ni**.

Characterization. Inductively coupled plasma optical emission spectroscopy (ICP-OES) was conducted on an Agilent 5100 ICP-OES, operated in Radical mode. A small piece of each material (<100 mg) was dissolved in 10 mL of 10% HCl at room temperature overnight. Upon complete dissolution of the sample, the solution turned green. Next, the solution was filtered by a 0.45 μm pore size polyethylene syringe filter. The filtered sample was transferred into a 10 mL tube. Nine standard samples were prepared for analysis, one blank and eight platinum standards in 10% HCl. Five typical wavelengths of Pt were also chosen, and all wavelengths were measured in triplicates. X-ray photoelectron spectroscopy (XPS) was obtained using a Thermo Scientific ESCALAB Xi^+ X-ray photoelectron spectrometer with an Al Kα X-ray source (1486.67 eV) and a spot size of 650 μm. The samples were loaded on carbon tape, and binding energies acquired were calibrated to the carbon C 1s C−C

https://doi.org/10.1021/acsami.3c08545
ACS Appl. Mater. Interfaces 2023, 15, 43756−43766

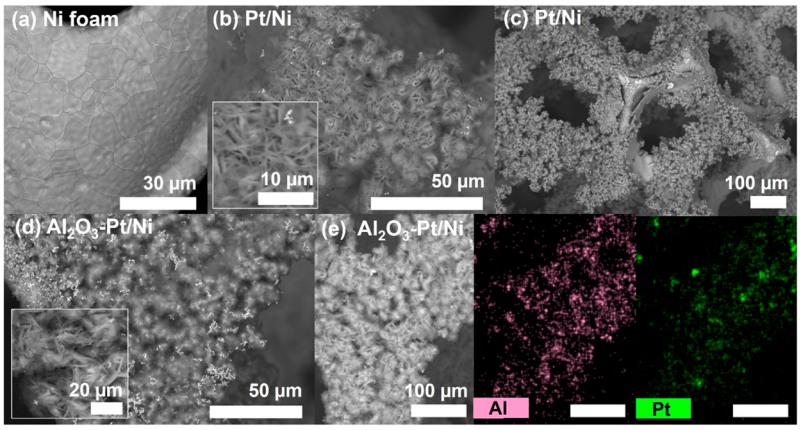

Figure 3. SEM micrographs of bare Ni foam (a), **Pt/Ni** (b, c), and **Al_2O_3-Pt/Ni** (d). SEM (c) micrograph highlighting surface delamination and degradation of **Pt/Ni**. SEM-EDS of **Al_2O_3-Pt/Ni** highlighting Al and Pt content (e).

peak at 284.8 eV. A pass energy of 20.0 eV was used with energy step sizes of 0.05 eV and 50 ms dwell times for the high-resolution spectra and step sizes of 0.5 eV with 20 ms dwell times for the survey scans. Survey spectra and high-resolution spectra are comprised of an average of three and eight scans, respectively. XPS peak fitting and analysis were performed with Thermo Scientific's Avantage Data System. Optical microscopy imaging was performed on an Olympus CX33 trinocular microscope with an Accu-Scope Excelis camera. Scanning electron microscopy (SEM) and energy dispersive X-ray spectroscopy (EDS) were obtained with a HITACHI tabletop microscope TM3000 and a QUANTAX 70 EDS from Bruker Nano. The samples were loaded on carbon tape for imaging. Conventional transmission electron microscopy (TEM), high resolution transmission electron microscopy (HR-TEM), high-angle annular dark-field scanning transmission electron microscopy (HAADF-STEM) with EDS, and selected area electron diffraction (SAED) pattern collection was performed at the Argonne chromatic aberration-corrected TEM. The SAED pattern simulations were carried out using Pierre Stadelmann's JEMS electron microscopy simulation software, and electron energy loss spectroscopy (EELS) analysis was carried out using Gatan Microscopy Suite (Digital Micrograph). BET surface area and pore size distribution were determined on a Quantachrome Autosorb-iQ physisorption chemisorption instrument. Prior to testing, the samples were outgassed at 300 °C for 1 h to remove all adsorbed molecules from the surface, and the nitrogen adsorption−desorption isotherm was measured using pressure intervals of $0 < P/P_0 < 1$ with 20 adsorption steps and 20 desorption steps. BET surface areas were calculated by using adsorption points in the relative pressures between 0.05 and 0.3. The nonlocal density functional theory (DFT) method was used to determine pore size distribution of the samples. Proton nuclear magnetic resonance (^{1}H NMR) spectroscopy measurements were conducted on a Bruker Avance III HD 400 MHz spectrometer, and all the data were analyzed using Mestrelab Research MestReNova.

General Procedure for Catalytic Hydrogenation Reactions. Hydrogenation reactions were performed in a 25 mL Büchiglasuster tinyclave glass reactor. Generally, the reactor was charged with substrate, catalyst, and absolute ethanol as solvent. The reactor was evacuated and quickly filled with ultrahigh purity H_2 gas. Next, the reaction mixture was heated in an oil bath under stirring to the desired temperature. After completion of the reaction, the reactor was cooled down to room temperature and the remaining H_2 was vented. The catalyst was removed physically with tweezers and washed with ethanol and DI water (for subsequent recycling for relevant reactions). Catalysts that were saved for recycling trials were dried in an oven at 150 °C under air. To perform product analysis, the ethanol in the reaction mixture was removed under reduced pressure via standard rotary evaporation to afford the product mixture. The product mixture was dissolved in $CDCl_3$ and analyzed by ^{1}H NMR spectroscopy.

RESULTS AND DISCUSSION

To fabricate supported Pt catalysts, precut and cleaned commercial Ni foams were hydrothermally reacted with $H_2PtCl_6{\cdot}6H_2O$ (chloroplatinic acid) in DI water. The process was accompanied by a color change in the solution from dark amber (dissolved chloroplatinic acid) to pale green, commensurate with the galvanic exchange of Pt^{4+} to Ni^{2+} in solution with concomitant deposition of Pt on the foam surface (Figure S1). The mechanism of Pt nanoparticle growth and nucleation using chloroplatinic acid in solution has been well-studied.[33−36] It is postulated that in parallel to the galvanic exchange process which seeds Pt on the Ni foam surface, a separate nucleation and growth process occurs to create Pt particles in solution. Some of these particles may nucleate to the surface-bound Pt and continue to grow particulates on the surface, while others likely remain in solution to be washed away upon workup (*vide infra*). The foams were worked-up according to the process detailed in the Experimental Section. Half of the foams were annealed under lab atmosphere to be used as control. The other half were treated with a thin Al_2O_3 overcoat via a thermal ALD process using DI water and TMA as co-reactants, consistent with the growth of a 2.17 nm film according to in situ spectroscopic ellipsometry. The resulting ALD-coated foams were annealed under lab atmosphere at 400 °C for 1 h (Figure 1). The two materials are labeled **Pt/Ni** and **Al_2O_3-Pt/Ni**, respectively. ICP-OES analysis of the two materials, as digested in HCl solution, revealed Pt concentrations of 0.27 ppm (**Pt/Ni**) and 0.020 ppm (**Al_2O_3-Pt/Ni**). Notably, **Pt/Ni** left a fine residue after handling (*vide infra*), indicating that a significant amount of surface material was lost during the requisite handling for the ALD process, resulting in the lower Pt concentration observed for **Al_2O_3-Pt/Ni**.

Pt/Ni and **Al_2O_3-Pt/Ni**, along with a bare Ni foam control, were initially imaged by transmitted light optical microscopy (Figure 2a−c). It was immediately evident that the fabrication process causes significant changes to the material structure; in both cases, the otherwise smooth Ni foam becomes conformally coated with "fuzzy" surface features. Notably, **Pt/Ni** and **Al_2O_3-Pt/Ni** bear distinguishing characteristics, **Al_2O_3-Pt/Ni** is darker, and the conformality of the surface features remains uninterrupted, whereas **Pt/Ni** features zones of discontinuity where it appears the surface is delaminating from the Ni foam core (Figure 2b).

https://doi.org/10.1021/acsami.3c08545
ACS Appl. Mater. Interfaces 2023, 15, 43756−43766

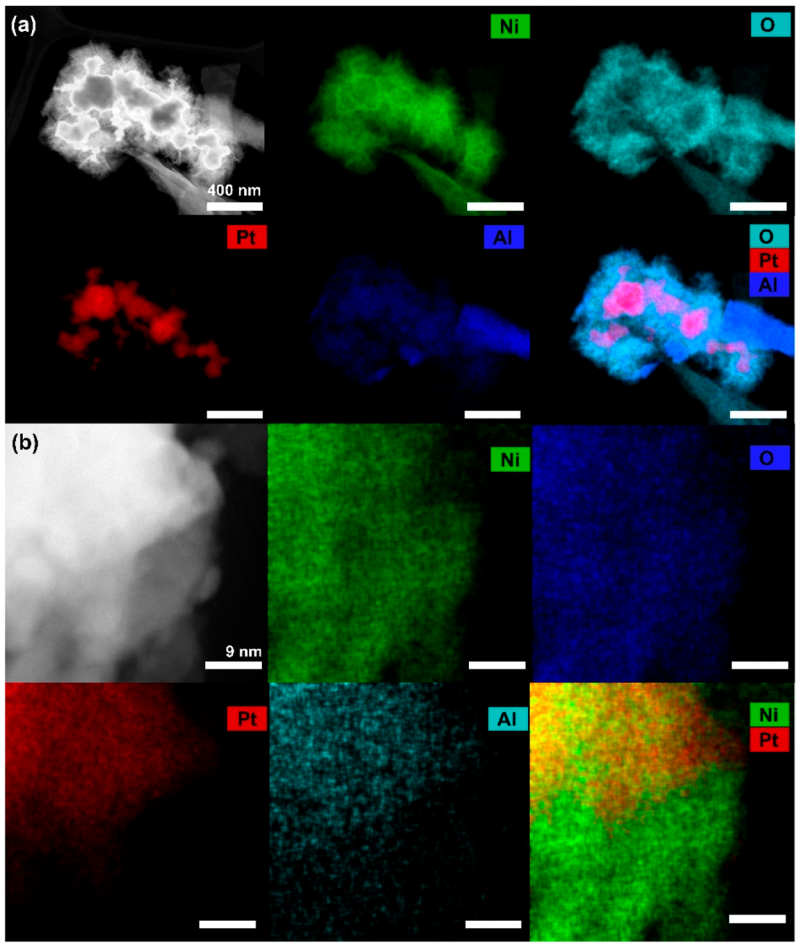

Figure 4. HAADF-STEM EDS of **Al_2O_3-Pt/Ni** showing the large sheet-like Pt aggregate (a) and a close up of the edge of the Pt region (b).

SEM provided a significantly more detailed view (Figure 3). Both **Pt/Ni** and **Al_2O_3-Pt/Ni** feature vertically oriented, densely packed nano-to-micro plates on the surface (Figure 3b–d). Such features have been previously reported for Ni-foam-based systems and are attributed to the formation of NiO_x nanosheets. The formation of these surface features is promoted by the acidic growth environment facilitated by the chloroplatinic acid precursor. A control reaction where Ni foam was treated with HCl and in the absence of Pt precursor led to similar surface features (Figures S2 and S3). Clustered Pt/PtO_x was not distinctly observable on the micrometer scale for **Pt/Ni** and **Al_2O_3-Pt/Ni**. The noted discontinuity in coverage and delamination for **Pt/Ni** can be clearly seen in Figure 3c, and it is readily observable over multiple samples. Further evidence of the fragility of **Pt/Ni** is noted during application where residue of **Pt/Ni** is sedimented after catalytic reaction (*vide infra*); similar physical degradation was not observed for **Al_2O_3-Pt/Ni**. This suggests that the ALD Al_2O_3 overcoat is also critical for the physical integrity of the NiO_x nanostructures formed during the materials synthesis process (*vide infra*). The utility of ALD Al_2O_3 protective overcoatings has been previously described in the literature;[37−39] thus it is not surprising that an observable impact is noted herein. SEM-EDS of **Al_2O_3-Pt/Ni** (Figures 3e and S4) confirmed a sparse distribution of Pt, with no significant clustering, and a conformal coating of Al_2O_3. The sparse Pt distribution is similarly noted for **Pt/Ni** (Figure S5) and is commensurate with the low loadings measured by ICP-OES.

To elucidate the nature of the surface structure of **Al_2O_3-Pt/Ni**, the nanoplates were mechanically removed by scraping with a stainless steel blade and loading the residue on a lacey carbon/Cu TEM grid. The samples were measured by both conventional TEM and HAADF-STEM with EDS (Figures 4, 5, and S6). Analysis of numerous nanoplates and aggregates revealed only a sparse population of Pt based material. The nature of the Pt particles appears as sheet-like clusters in the 50−300 nm diameter range (Figure 4a). While it cannot be discounted for the entirety of the sample, no evidence of large aggregate growth in the *z*-direction was observed, implying that the Pt particles grow preferentially along the Ni-foam

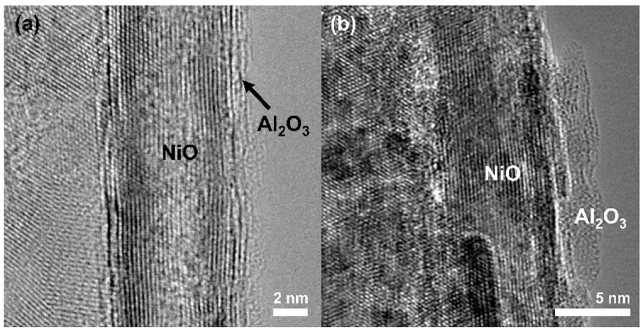

Figure 5. Edge-on HR-TEM micrographs highlighting the Al_2O_3 overcoat (a, b).

https://doi.org/10.1021/acsami.3c08545
ACS Appl. Mater. Interfaces 2023, 15, 43756−43766

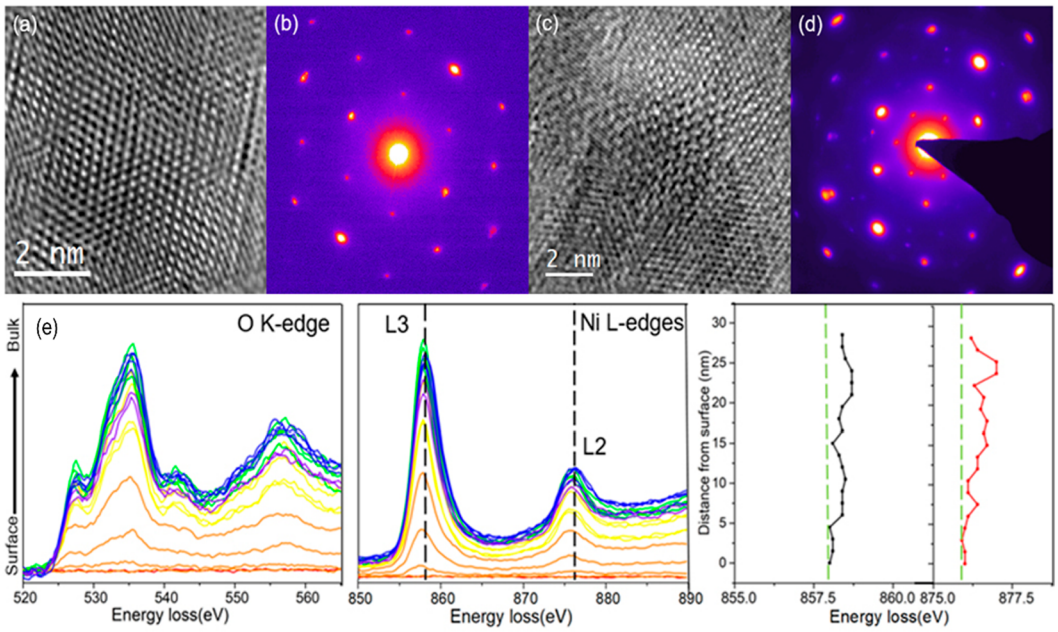

Figure 6. SAED and EELS analysis of the NiO/Ni_2O_3 superstructure. (a, b) High-resolution image of the NiO region and the corresponding SAED pattern. (c, d) High-resolution image of the region with a superstructure domain and the corresponding SAED pattern. The extra spots were used to match with the simulated Ni_2O_3 SAED pattern. (e) EELS linescan analysis and the corresponding O and Ni edges. As seen in the figure, the shift position is not completely uniform, indicating that the superstructure domains are scattered on the outmost surface of the sample.

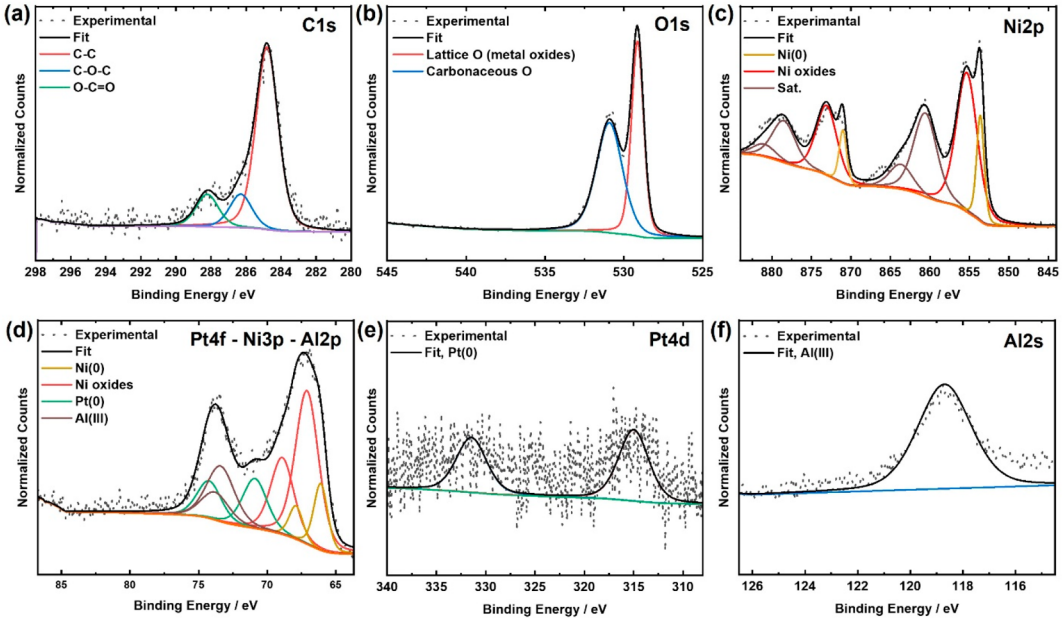

Figure 7. High resolution X-ray photoelectron spectroscopy of **Al_2O_3-Pt/Ni** (a−f).

surface. Higher resolution imaging at the edge of the Pt particle domain revealed a gradient of Pt to Ni (Figure 4b), consistent with a galvanic exchange process. Careful analysis at high resolution of the nanoplate surfaces did not show any evidence of single atom Pt domains separate from the periphery of the noted sheet-like aggregates. EDS analysis of Al was consistent with a conformal coating of Al_2O_3 via the ALD process. The higher intensity O signal is consistent with O atoms from both Al_2O_3 and the NiO comprising the bulk of the nanoplates. High resolution TEM of the general Al_2O_3 coated NiO domains (excluding the sparse Pt regions) was consistent with a thin, conformal approximately <2 nm layer of Al_2O_3 (Figures 5 and S7), exhibiting both monocrystalline (Figure 5a) and pseudomonocrystalline domains (Figure 5b).

During the TEM observation of the surface regions, superstructure spots appeared on the SAED pattern of the region of interest (Figure 6a−d). In order to analyze the phenomena, diffraction simulations were carried out, as well as EELS analysis. The diffraction pattern matching revealed the superstructure to be Ni_2O_3. However, the uniformity of the superstructure came into question. In order to further analyze the phenomena, EELS linescans were conducted over the

https://doi.org/10.1021/acsami.3c08545
ACS Appl. Mater. Interfaces 2023, 15, 43756−43766

regions with superstructure presence (Figure 6e). After careful analysis of the Ni L-edges, there is a noticeable chemical shift from Ni^{3+} to Ni^{2+}, further supporting the results of the diffraction analysis. The shift, however, was not uniform throughout the linescan area; thus, it was concluded that the Ni_2O_3 domains are not uniformly distributed throughout the surface regions of the sample but rather form a superstructure with NiO in some regions toward the outermost surface.

BET surface area measurements were performed on **Pt/Ni** and **Al_2O_3-Pt/Ni**. The corresponding surface areas were 3.5 m^2g^{-1} for **Pt/Ni** and 5.2 m^2g^{-1} for **Al_2O_3-Pt/Ni**, whereas bare Ni foam is typically ~1 m^2 g^{-1}.[40] Respective average pore diameters were 2.7 nm for **Pt/Ni** and 2.9 nm for **Al_2O_3-Pt/Ni** (Figure S8). These are consistent with the formation of NiO nanoplates compared to the lower value for unreacted Ni foam. The enhanced surface area for **Al_2O_3-Pt/Ni** is associated with the presence of porosity in the Al_2O_3 overcoat.[29]

X-ray photoelectron spectroscopy (XPS) was carried out to identify the surface composition and valence states of the elements in the prepared materials (Figure 7). The survey scan of **Al_2O_3-Pt/Ni** indicates the presence of Ni, O, C, Pt, and Al (Figure S9). The C 1s region was fitted to three peaks at binding energies (BE) of 284.8, 286.3, and 288.2 eV that are attributed to C−C/C═C, C−O−C, and O−C═O species, respectively (Figure 7a).[41] The O 1s spectrum was fitted to two peaks at the BE of 529.1 and 530.9 eV attributed to the lattice oxygen of Ni- and Al-oxides and adsorbed oxygen, respectively (Figure 7b).[41−43] The high-resolution Ni 2p spectrum can be deconvoluted into two doublet peaks (Figure 7c). The Ni $2p_{3/2}$ peak at 853.6 eV is assigned to Ni(0), and the broad component at 855.3 eV is assigned to Ni-oxides, NiO and Ni_2O_3.[44−46] The BE appears to be red-shifted compared to that reported for Ni_2O_3 and slightly blue-shifted from that of NiO, commensurate with an NiO- and Ni_2O_3-passivated surface, with some regions of subsurface metallic Ni. These observations are consistent with the TEM and EELS analysis that Ni_2O_3 species are present but not uniformly distributed throughout the surface regions.

The Pt 4f region (64−86 eV) overlaps with Ni 3p and Al 2p and can be fitted into four doublets (Figure 7d). The peaks at 66.1 and 67.1 eV correspond to the BE of Ni $3p_{3/2}$ for metallic Ni and Ni oxides, respectively. The signal was also fitted to a doublet centered at 70.9 eV with a splitting of 3.3 eV commensurate with the BE of Pt $4f_{7/2}$ peak for Pt(0).[47] The peak at 73.4 eV is attributed to the Al 2p transition in Al_2O_3.[48,49] Due to the complexity of this region, Pt 4d and Al 2s spectra were also obtained. The Pt 4d transition is an order of magnitude weaker than the corresponding Pt 4f and was fitted to a doublet peak centered at 315.0 eV for the $4d_{5/2}$ peak, further indicating the presence of Pt(0) (Figure 7e).[47,50] The low signal-to-noise is attributed to the ultralow loading of Pt, as determined by ICP-OES (~0.02 ppm, *vide supra*). Lastly, the Al 2s spectrum was fitted to a peak centered at 118.7 eV, confirming the presence of single phase Al_2O_3 (Figure 7f).[48,49] Notably, XPS scans of separate batches of **Al_2O_3-Pt/Ni**, fabricated months apart, appear very similar, validating the general reproducibility of this process (Figure S11).

To establish the catalytic activity for **Al_2O_3-Pt/Ni**, the hydrogenation of styrene was studied (Figure 8a). To build a time profile, individual experiments were conducted at 2, 4, 8, 12, 14, 16, 18, and 24 h time points utilizing different pieces of **Al_2O_3-Pt/Ni** of similar weight (62.52 ± 1.44 mg; approximately 12 mm × 12 mm × 1.6 mm). Utilizing a previously

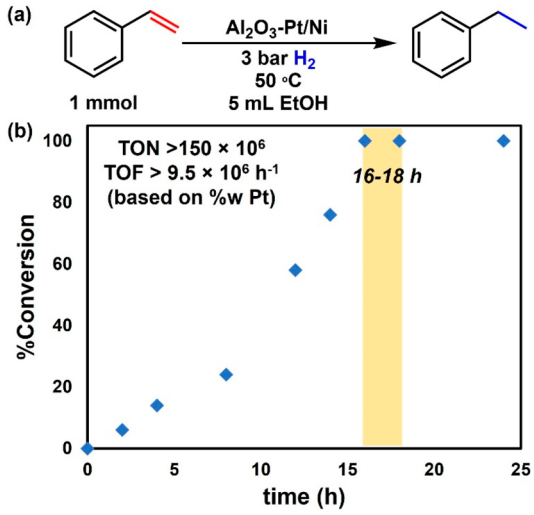

Figure 8. Reaction scheme for the catalytic hydrogenation of styrene utilizing the **Al_2O_3-Pt/Ni** catalyst (a). Conversion vs time for the catalytic hydrogenation of styrene utilizing **Al_2O_3-Pt/Ni** catalyst with 1 mmol of styrene and 3 bar of H_2 gas at 50 °C (b). Each data point represents an individual trial with a new piece of catalyst of similar mass, showcasing the consistency in the material. Reaction reaches 100% conversion at the 16−18 h time points.

reported mild hydrogenation protocol,[15] reactions were conducted at 3 bar of H_2 with 5 mL of EtOH at 50 °C and 1 mmol styrene. Full conversion to ethylbenzene was achieved at the 16−18 h time points (Figures 8b and S14). To validate that the reactivity was due to Pt, control trials were conducted under identical conditions, first with no catalyst and with similar loadings of 400 °C annealed Ni foam, HCl treated Ni foam, and Al_2O_3 coated Ni foam. Under all control conditions, no styrene hydrogenation or other reactions were observed (Figure S15), confirming that the support and overcoat are inert under the reaction conditions tested and the catalytic activity is due solely to Pt. Due to the inherent heterogeneity of the catalyst framework and complexity of the surface features, conventional analysis of turnover frequency (TOF) becomes difficult. However, a more conservative gravimetric approach based on mol styrene/mol Pt in the system can be used to generate what is likely an underestimated TOF of 9.5 × 10^6 h^{-1} (average between the 16 and 18 h trials), a high value owing to the ultralow 0.020 ppm loading of Pt. This compares very favorably with some of the fastest styrene hydrogenation systems reported in the literature: ALD Pt/CNTs, ~1.25 × 10^4 h^{-1} (25 °C, 30 bar of H_2);[11] amidinate coated Pt NPs, 7.53 × 10^4 h^{-1} (60 °C, 5 bar of H_2);[10] Pt/PO_4-CeO_2, 316 h^{-1} (60 °C, 1 bar of H_2);[51] Pd/Pr_6O_{11}, 8.96 × 10^3 h^{-1} (25 °C, 1 bar of H_2);[52] Pd_1/TiO_2, 8.97 × 10^3 h^{-1} (30 °C, 1 bar of H_2).[53]

To demonstrate the reusability of **Al_2O_3-Pt/Ni** and validate the material design choices compared to **Pt/Ni**, 10 consecutive hydrogenations of styrene were conducted. Reaction parameters were chosen to reflect standard reaction conditions of 1 mmol of styrene, catalyst weight reflecting ~2 × 10^{-6} mg of Pt for **Al_2O_3-Pt/Ni** and ~4 × 10^{-6} mg of Pt for **Pt/Ni** (to reach 100% conversion on run 1), 4 bar of H_2, in 5 mL of EtOH at 50 °C for a reaction time of 24 h. After each cycle, the catalysts were physically removed with tweezers and washed with ethanol and DI water, then dried at 150 °C in a standard lab oven under ambient atmosphere. No special precautions were

https://doi.org/10.1021/acsami.3c08545
ACS Appl. Mater. Interfaces 2023, 15, 43756−43766

undertaken to sediment, separate, or reuse any residual material; thus physical damage to the catalysts should reflect in loss to reactivity. In over 10 consecutive catalysis and washing/handling sequences, only 4% loss in conversion, with no impact on selectivity, was observed for **Al_2O_3-Pt/Ni** (Figures 9a and S16). By contrast, **Pt/Ni** performed far worse over the 10 trials (Figures 9b and S17). Spent **Al_2O_3-Pt/Ni** was analyzed by ICP-OES and was found to contain 0.017 ppm of Pt. Considering the natural inhomogeneity of these materials, the difference from the fresh material (0.020 ppm Pt) is minimal. When factoring in the retention of catalytic activity, it is likely that the catalyst is not significantly deteriorated. Optical microscopy, SEM-EDS, and TEM measurements corroborate the integrity of the physical structure of the material (Figures S18−S21). XPS of the spent material reveals a lower intensity Pt peak, with a Pt 4f that can be better fitted to Pt(II) (commensurate with PtO formation), and evolution of C 1s and O 1s signals that can be attributed to adsorbed organics (Figure S22). Notably the spent catalyst was not cleaned prior to measurement; thus formation of a thin surface oxide and the presence of residual organics are expected.

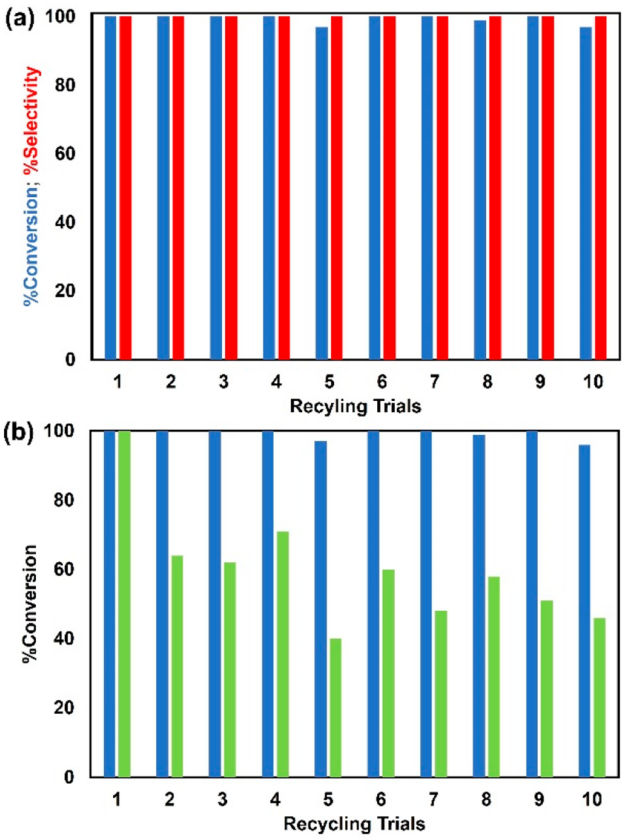

Figure 9. Catalyst recycling trials for the hydrogenation of styrene using a modified protocol to Figure 8a; 1 mmol of styrene, 103.5 mg of **Al_2O_3-Pt/Ni** (∼2×10^{-6} mg of Pt), 4 bar of H_2, 50 °C, 24 h, and 5 mL of EtOH (a). Comparison of catalyst recycling behavior for **Al_2O_3-Pt/Ni** (blue) with **Pt/Ni** (green) under conditions noted in part a, with ∼4×10^{-6} mg of Pt for **Pt/Ni** (b); notably, the selectivity remained unchanged for both **Al_2O_3-Pt/Ni** and **Pt/Ni**.

Concomitantly, while **Pt/Ni** reached 100% conversion for trial 1, it dropped markedly to 64% conversion in trial 2 and down to 46% conversion by trial 10. The dramatic decrease in reactivity is attributed to the physical deterioration of the material, which was evident as fine dark residue could be observed in the reactor, especially after the first trial (Figure S23). Because **Pt/Ni** proved to be too fragile, it was not studied further. In all cases (both **Pt/Ni** and **Al_2O_3-Pt/Ni**), selectivity appeared to be unaffected, favoring only ethylbenzene as the hydrogenation product. These results validate the materials design choices made for the preparation of **Al_2O_3-Pt/Ni**, namely, the ultrathin ALD Al_2O_3 overcoat, which has shown remarkable impact in maintaining catalyst reactivity and physical integrity over extended recycling. In this case, it is likely the ALD overcoat is preventing loss of Pt particles by physical encapsulation and appears to be aiding in the overall physical integrity of the support surface nanostructure (*vide supra*). Moreover, the role of selective ALD overcoating cannot be discounted in enhancing catalyst performance. Dameron, Nicholas, Marshall, and co-workers have previously noted improved catalyst selectivity and longevity for ALD Al_2O_3 overcoated Pt catalysts for propane dehydrogenation.[28] ALD nucleation and growth were speculated to occur preferentially at undercoordinated sites, leaving more selective terrace sites accessible. This phenomenon may be used to explain the remarkable tolerance for multiple functional groups displayed by **Al_2O_3-Pt/Ni** (*vide infra*).

With the validated best catalyst in hand, **Al_2O_3-Pt/Ni**, the substrate scope was expanded to eight other styrene derivatives (Scheme 1a−j and Figures S24−S33). In general, good-to-excellent conversions were observed over a range of functional groups in the *para* position, with complete selectivity toward the ethylbenzene derivative in all but one case. Notably, there was complete tolerance toward *para*-Br, Cl, and CF_3 functionalities (Scheme 1b−d), with complete conversion being achieved for *para*-CF_3 (Scheme 1d). The presence of *ortho* substituents (Scheme 1g) significantly lowered the reactivity, likely due to steric implications. *Para*-NO_2 was quantitatively hydrogenated at both the vinyl and nitro functionalities yielding 4-ethylaninline (Scheme 1f), indicating strong reactivity toward both groups under the conditions tested. Repeating the latter reaction at 21 °C and half the substrate loading lowered the conversion to ∼56%, with 93% selectivity toward the 4-ethylnitrobenzene (Scheme 1g) product. This is indicative of preferential hydrogenation of the vinyl group and highlights the potential for temperature-mediated selectivity. At a lower reaction temperature of 30 °C, hydrogenation of phenylacetylene derivatives was also attempted (Scheme 1k−m and Figures S34−S36). Complete conversion of phenylacetylene (Scheme 1k) was readily achieved, with ∼74% selectivity toward styrene and with the remaining product as ethylbenzene. *Para* F and Cl variants (Scheme 1l,m) were also tested with good-to-excellent conversions and similar selectivity toward the styrene. In the latter, there was no reactivity toward the halogen groups. As expected, the system continues reacting to hydrogenate the vinyl group; however, the overall selectivity is reasonable and may be improved further by lowering the reaction temperature or implementing a flow process.

Tolerance toward hydrodehalogenation is attributed to the preferential Al_2O_3 overcoating of undercoordinated Pt sites, leaving predominantly terraces available for reactivity. Li et al. report a strong preference for hydrodehalogenation of halonitrobezenes and halonitroamines at Pd nanoparticle edges over terraces;[54] a similar phenomenon is attributed to the Pt catalysts reported herein. Selectivity toward semi-

https://doi.org/10.1021/acsami.3c08545
ACS Appl. Mater. Interfaces 2023, 15, 43756−43766

Scheme 1. Scope of Catalytic Hydrogenation of Styrene (a–j) and Phenylacetylene (k–m) Derivatives Utilizing 66.84 ± 7.55 mg Piece of Al_2O_3-Pt/Ni Catalyst[a]

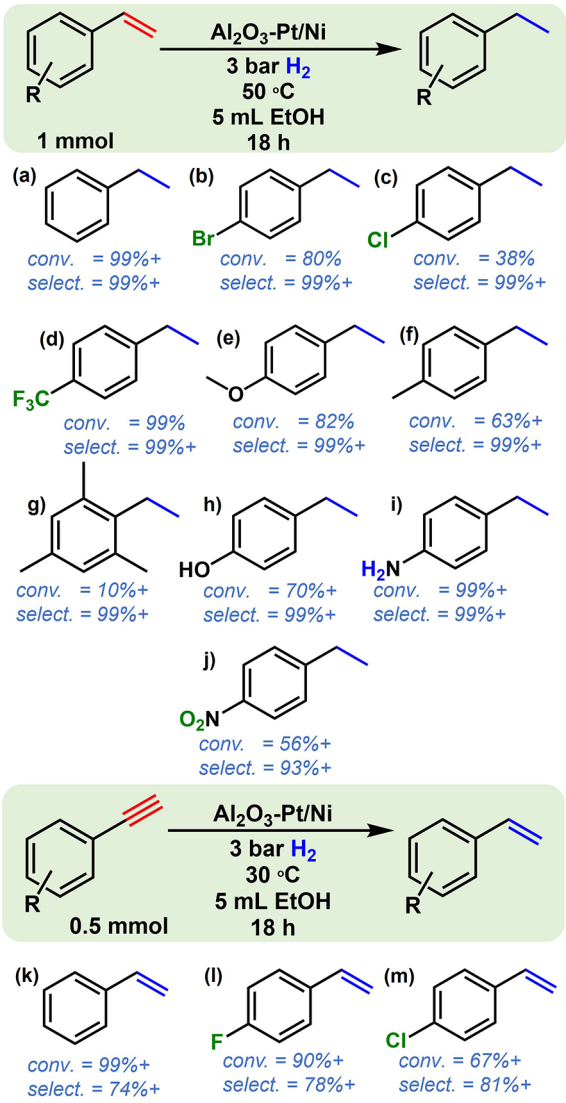

[a]Modifications to the reaction conditions: g = 0.4 mmol, 4 bar; j = 0.5 mmol, 21 °C, k = 1 mmol, 4 bar.

hydrogenation of phenylacetylene derivatives is attributed to weaker surface interaction of the alkene vs the alkyne. Al_2O_3 coverage of undercoordinated and more reactive sites such as edges, corners, or defects is anticipated to impact the binding of the alkene.[55] Combined with the decrease in reaction temperature (30 °C vs 50 °C), the system becomes biased toward preferential semihydrogenation of alkynes even at high conversion. As noted, at 50 °C, **Al_2O_3-Pt/Ni** is remarkably active toward styrene hydrogenation. Electronic metal–support interactions (EMSI) are expected to play a role and have been shown to significantly contribute to the selectivity of Pt toward alkyne semihydrogenation[56] and additionally toward halogen tolerance.[57] The interaction of Pt with NiO_x and Al_2O_3 is anticipated to create partial $Pt^{\delta+}$ sites, which can alter the styrene surface interaction, leading to weaker binding. A detailed examination of BEs from the XPS analysis is hampered by the ultralow loading of Pt which creates poor signal to noise in the Pt 4d region and significant overlap with Ni 3p and Al 2s in the Pt 4f region. Annecdotally, Pt^0 was fitted to a BE of 70.1 eV (Figure S10) for Pt/Ni and 70.9 eV (Figure 7d) for **Al_2O_3-Pt/Ni**, implying a more electron deficient state of Pt and creation of $Pt^{\delta+}$ sites. The attribution of selectivity to modifications of the Pt surface is based on the presumption of a Horiuti–Polanyi type mechanism.[58,59] However, the potential role or presence of a hydrogen spillover mechanism cannot be discounted.[32]

CONCLUSIONS

In summary, a Ni foam-supported Pt catalyst system with ultralow loading of noble metal was prepared and stabilized with an ultrathin coating of ALD Al_2O_3, with subsequent annealing (**Al_2O_3-Pt/Ni**). In addition to stabilizing the Pt particles on the surface, the ~2 nm Al_2O_3 overcoat contributes to the overall structural integrity of the NiO_x nanoplates, which grow on the Ni foam surface and also serve as support for the Pt. Increased robustness is immediately observed by enhanced physical integrity of the monolith material and subsequently in the retention of catalytic activity over 10 standard catalyst recycling trials, both in marked contrast to the uncoated samples. Catalyst activity was validated via the hydrogenation of various functionalized styrene and phenylacetylene derivatives, where **Al_2O_3-Pt/Ni** displayed excellent activity and functional group tolerance toward halides, all under mild and sustainable reaction conditions. To the best of our knowledge, this is the first example of thermal hydrogenation catalysis with a Ni foam-supported Pt catalyst and one of the highest TOFs reported for the ubiquitous styrene hydrogenation reaction. Ongoing efforts focus on enhancing the control over Pt particle size and distribution and expanding catalytic reactivity and scope.

ASSOCIATED CONTENT

Supporting Information

The Supporting Information is available free of charge at https://pubs.acs.org/doi/10.1021/acsami.3c08545.

Images of color change during deposition of Pt on the foam surface, SEM micrograph and corresponding EDS of HCl etched Ni foam, Al_2O_3-Pt/Ni, and Pt/Ni, BET of Pt/Ni and Al_2O_3-Pt/Ni, XPS spectra of Pt/Ni, Al_2O_3-Pt/Ni, and spent Al_2O_3-Pt/Ni, optical, SEM and TEM micrographs of spent Al_2O_3-Pt/Ni, and ^{1}H NMR spectra of the hydrogenation products (PDF)

AUTHOR INFORMATION

Corresponding Authors

Jianguo Wen – *Center for Nanoscale Materials, Argonne National Laboratory, Lemont, Illinois 60439, United States;* orcid.org/0000-0002-3755-0044; Email: jwen@anl.gov

Titel Jurca – *Department of Chemistry, University of Central Florida, Orlando, Florida 32816, United States; NanoScience and Technology Center (NSTC), University of Central Florida, Orlando, Florida 32826, United States; Renewable Energy and Chemical Transformation Faculty Cluster (REACT), University of Central Florida, Orlando, Florida 32816, United States;* orcid.org/0000-0003-3656-912X; Email: titel.jurca@ucf.edu

Authors

Azina Rahmani – *Department of Chemistry, University of Central Florida, Orlando, Florida 32816, United States*

https://doi.org/10.1021/acsami.3c08545
ACS Appl. Mater. Interfaces 2023, 15, 43756–43766

Maksim A. Sultanov − *Center for Nanoscale Materials, Argonne National Laboratory, Lemont, Illinois 60439, United States; Department of Physics, Northern Illinois University, DeKalb, Illinois 60115, United States*

Kemah Kamiru-White − *Department of Chemistry, University of Central Florida, Orlando, Florida 32816, United States*

Lorianne R. Shultz-Johnson − *Department of Chemistry, University of Central Florida, Orlando, Florida 32816, United States*

Brian E. Butkus − *Department of Materials Science and Engineering, University of Central Florida, Orlando, Florida 32816, United States*

Shaohua Xie − *Department of Civil, Environmental, and Construction Engineering, University of Central Florida, Orlando, Florida 32816, United States;* orcid.org/0000-0003-1550-7421

Fudong Liu − *Department of Civil, Environmental, and Construction Engineering and Renewable Energy and Chemical Transformation Faculty Cluster (REACT), University of Central Florida, Orlando, Florida 32816, United States; NanoScience and Technology Center (NSTC), University of Central Florida, Orlando, Florida 32826, United States;* orcid.org/0000-0001-8771-5938

Diep T. H. Nguyen − *Department of Chemistry, NanoQAM, Quebec Centre for Advanced Materials, Université du Québec à Montréal, Montréal, QC H3C 3P8, Canada*

Noémie Wilson-Faubert − *Department of Chemistry, NanoQAM, Quebec Centre for Advanced Materials, Université du Québec à Montréal, Montréal, QC H3C 3P8, Canada*

Ali Nazemi − *Department of Chemistry, NanoQAM, Quebec Centre for Advanced Materials, Université du Québec à Montréal, Montréal, QC H3C 3P8, Canada;* orcid.org/0000-0002-6504-582X

Parag Banerjee − *Department of Materials Science and Engineering and Renewable Energy and Chemical Transformation Faculty Cluster (REACT), University of Central Florida, Orlando, Florida 32816, United States; NanoScience and Technology Center (NSTC), University of Central Florida, Orlando, Florida 32826, United States;* orcid.org/0000-0003-0401-8155

Lei Zhai − *Department of Chemistry, University of Central Florida, Orlando, Florida 32816, United States; Department of Materials Science and Engineering, University of Central Florida, Orlando, Florida 32816, United States; NanoScience and Technology Center (NSTC), University of Central Florida, Orlando, Florida 32826, United States;* orcid.org/0000-0002-3886-2154

Massimiliano Delferro − *Chemical Sciences and Engineering Division, Argonne National Laboratory, Lemont, Illinois 60439, United States;* orcid.org/0000-0002-4443-165X

Complete contact information is available at: https://pubs.acs.org/10.1021/acsami.3c08545

Author Contributions

A. Rahmani: investigation, methodology, formal analysis, writing—original draft, writing—reviewing and editing. M. A. Sultanov: investigation, formal analysis, writing—original draft, writing—reviewing and editing. K. Kamiru-White: investigation, formal analysis. L. R. Shultz-Johnson: investigation, formal analysis. B. E. Butkus: investigation, formal analysis. S. Xie: investigation, formal analysis. F. Liu: resources. D. T. H. Nguyen: investigation, writing—reviewing and editing. N. Wilson-Faubert: investigation, writing—reviewing and editing. A. Nazemi: supervision, writing—reviewing and editing. P. Banerjee: supervision, writing—original draft, writing—reviewing and editing. L. Zhai: supervision, writing—reviewing and editing. M. Delferro: formal analysis, project administration, writing—reviewing and editing. J. Wen: supervision, methodology, conceptualization, formal analysis, project administration, funding acquisition, writing—original draft, writing—reviewing and editing. T. Jurca: supervision, methodology, conceptualization, formal analysis, project administration, funding acquisition, writing—original draft, writing—reviewing and editing.

Funding

The authors thank NSF Award 2121953 and the PREM Center for Ultrafast Dynamics and Catalysis in Emerging Materials for partially supporting this work.

Notes

The authors declare no competing financial interest.

ACKNOWLEDGMENTS

L.R.S.-J. thanks the Ford Foundation for a Dissertation Fellowship. T.J. thanks the Department of Chemistry, College of Sciences, and the FCI at the University of Central Florida. M.D. at Argonne National Laboratory acknowledges the U.S. DOE, Office of Basic Energy Sciences, Division of Chemical Sciences, Geosciences, and Biosciences, Catalysis Science Program, under Contract DE-AC02-06CH11357. The authors also acknowledge the NSF MRI: ECCS: 1726636 and MCF-AMPAC facility. Work performed at the Center for Nanoscale Materials, a U.S. Department of Energy Office of Science User Facility, was supported by the U.S. DOE, Office of Basic Energy Sciences, under Contract DE-AC02-06CH11357. A.N. thanks the Natural Sciences and Engineering Research Council of Canada (NSERC) Grant RGPIN-2018-05799.

ABBREVIATIONS

ALD = atomic layer deposition
SEM = scanning electron microscopy
TEM = transmission electron microscopy
HAADF-STEM = high-angle annular dark-field scanning transmission electron microscopy
XPS = X-ray photoelectron spectroscopy
BET = Brunauer, Emmett, and Teller

REFERENCES

(1) Zhu, L.; Wang, L.-S.; Li, B.; Li, W.; Fu, B. Methylation of Aromatic Amines and Imines using Formic Acid over a Heterogeneous Pt/C Catalyst. *Catal. Sci. Technol.* **2016**, *6* (16), 6172−6176.

(2) Lee, I.; Morales, R.; Albiter, M. A.; Zaera, F. Synthesis of Heterogeneous Catalysts with Well Shaped Platinum Particles to Control Reaction Selectivity. *Proc. Natl. Acad. Sci. U. S. A.* **2008**, *105* (40), 15241−15246.

(3) Tian, S.; Wang, B.; Gong, W.; He, Z.; Xu, Q.; Chen, W.; Zhang, Q.; Zhu, Y.; Yang, J.; Fu, Q.; et al. Dual-Atom Pt Heterogeneous Catalyst with Excellent Catalytic Performances for the Selective Hydrogenation and Epoxidation. *Nat. Commun.* **2021**, *12* (1), 3181.

(4) Mallat, T.; Baiker, A. Oxidation of Alcohols with Molecular Oxygen on Solid Catalysts. *Chem. Rev.* **2004**, *104* (6), 3037−3058.

(5) Cui, X.; Junge, K.; Dai, X.; Kreyenschulte, C.; Pohl, M.-M.; Wohlrab, S.; Shi, F.; Brückner, A.; Beller, M. Synthesis of Single Atom based Heterogeneous Platinum Catalysts: High Selectivity and Activity for Hydrosilylation Reactions. *CS Cent. Sci.* **2017**, *3* (6), 580−585.

(6) Li, K.; Qin, R.; Liu, K.; Zhou, W.; Liu, N.; Zhang, Y.; Liu, S.; Chen, J.; Fu, G.; Zheng, N. Carbon Deposition on Heterogeneous Pt Catalysts Promotes the Selective Hydrogenation of Halogenated Nitroaromatics. *ACS Appl. Mater. Interfaces* **2021**, *13* (44), 52193−52201.

(7) Shultz, L. R.; Hu, L.; Preradovic, K.; Beazley, M. J.; Feng, X.; Jurca, T. A Broader-Scope Analysis of the Catalytic Reduction of Nitrophenols and Azo Dyes with Noble Metal Nanoparticles. *ChemCatChem* **2019**, *11* (11), 2590−2595.

(8) Imaoka, T.; Akanuma, Y.; Haruta, N.; Tsuchiya, S.; Ishihara, K.; Okayasu, T.; Chun, W.-J.; Takahashi, M.; Yamamoto, K. Platinum Clusters with Precise Numbers of Atoms for Preparative-Scale Catalysis. *Nat. Commun.* **2017**, *8* (1), 688.

(9) Boualleg, M.; Norsic, S.; Baudouin, D.; Sayah, R.; Quadrelli, E. A.; Basset, J.-M.; Candy, J.-P.; Délichère, P.; Pelzer, K.; Veyre, L.; Thieuleux, C. Selective and Regular Localization of Accessible Pt Nanoparticles Inside the Walls of an Ordered Silica: Application as a Highly Active and Well-Defined Heterogeneous Catalyst for Propene and Styrene Hydrogenation Reactions. *J. Catal.* **2011**, *284* (2), 184−193.

(10) Martínez-Prieto, L. M.; Cano, I.; Márquez, A.; Baquero, E. A.; Tricard, S.; Cusinato, L.; Del Rosal, I.; Poteau, R.; Coppel, Y.; Philippot, K.; et al. Zwitterionic Amidinates as Effective Ligands for Platinum Nanoparticle Hydrogenation Catalysts. *Chem. Sci.* **2017**, *8* (4), 2931−2941.

(11) Li, J.; Zhang, B.; Chen, Y.; Zhang, J.; Yang, H.; Zhang, J.; Lu, X.; Li, G.; Qin, Y. Styrene Hydrogenation Performance of Pt Nanoparticles with Controlled Size Prepared by Atomic Layer Deposition. *Catal. Sci. Technol.* **2015**, *5* (8), 4218−4223.

(12) Jin, Y.; Wang, P.; Mao, X.; Liu, S.; Li, L.; Wang, L.; Shao, Q.; Xu, Y.; Huang, X. A Top-Down Strategy to Realize Surface Reconstruction of Small-Sized Platinum-Based Nanoparticles for Selective Hydrogenation. *Angew. Chem.* **2021**, *133* (32), 17570−17574.

(13) Hughes, A. E.; Haque, N.; Northey, S. A.; Giddey, S. Platinum group metals: A Review of Resources, Production and Usage with a Focus on Catalysts. *Resources* **2021**, *10* (9), 93.

(14) *Mineral Commodity Summaries 2023*; U.S. Geological Survey: Reston, VA, 2023; http://pubs.er.usgs.gov/publication/mcs2023, DOI: 10.3133/mcs2023.

(15) Rahmani, A.; Currie, T. M.; Shultz, L. R.; Bryant, J. T.; Beazley, M. J.; Uribe-Romo, F. J.; Tetard, L.; Rudawski, N. G.; Xie, S.; Liu, F.; Wang, T.-H.; Ong, T.-G.; Zhai, L.; Jurca, T. Robust Palladium Catalysts on Nickel Foam for Highly Efficient Hydrogenations. *Catal. Sci. Technol.* **2022**, *12* (23), 6992−6997.

(16) Shultz, L. R.; Preradovic, K.; Ghimire, S.; Hadley, H. M.; Xie, S.; Kashyap, V.; Beazley, M. J.; Crawford, K. E.; Liu, F.; Mukhopadhyay, K.; Jurca, T. Nickel Foam Supported Porous Copper Oxide Catalysts with Noble Metal-like Activity for Aqueous Phase Reactions. *Catal. Sci. Technol.* **2022**, *12* (12), 3804−3816.

(17) Giani, L.; Groppi, G.; Tronconi, E. Heat Transfer Characterization of Metallic Foams. *Ind. Eng. Chem. Res.* **2005**, *44* (24), 9078−9085.

(18) Dou, L.; Yan, C.; Zhong, L.; Zhang, D.; Zhang, J.; Li, X.; Xiao, L. Enhancing CO_2 Methanation Over a Metal Foam Structured Catalyst by Electric Internal Heating. *Chem. Commun.* **2020**, *56* (2), 205−208.

(19) Pentsak, E. O.; Eremin, D. B.; Gordeev, E. G.; Ananikov, V. P. Phantom Reactivity in Organic and Catalytic Reactions as a Consequence of Microscale Destruction and Contamination-Trapping Effects of Magnetic Stir Bars. *ACS Catal.* **2019**, *9* (4), 3070−3081.

(20) Milazzo, R. G.; Privitera, S. M.; D'Angelo, D.; Scalese, S.; Di Franco, S.; Maita, F.; Lombardo, S. Spontaneous Galvanic Displacement of Pt Nanostructures on Nickel Foam: Synthesis, Characterization and use for Hydrogen Evolution Reaction. *Int. J. Hydrog. Energy* **2018**, *43* (16), 7903−7910.

(21) Milazzo, R. G.; Privitera, S. M.; Scalese, S.; Lombardo, S. A. Effect of Morphology and Mechanical Stability of Nanometric Platinum Layer on Nickel Foam for Hydrogen Evolution Reaction. *Energies* **2019**, *12* (16), 3116.

(22) Van Drunen, J.; Pilapil, B. K.; Makonnen, Y.; Beauchemin, D.; Gates, B. D.; Jerkiewicz, G. Electrochemically Active Nickel Foams as Support Materials for Nanoscopic Platinum Electrocatalysts. *ACS Appl. Mater. Interfaces* **2014**, *6* (15), 12046−12061.

(23) Xiao, X.; Sun, D.; Liu, X.; Qiu, B.; Xu, X.; Zhang, D.; Yang, T. Ultra-Low Amount Pt-Doped Co_2P/Ni_2P on Nickel Foam as an Efficient Electrocatalyst for the Hydrogen Evolution Reaction in an Alkaline Electrolyte. *Sustain. Energy Fuels* **2021**, *5* (4), 1059−1066.

(24) Li, M.; Ma, Q.; Zi, W.; Liu, X.; Zhu, X.; Liu, S. Pt Monolayer Coating on Complex Network Substrate with High Catalytic Activity for the Hydrogen Evolution Reaction. *Sci. Adv.* **2015**, *1* (8), No. e1400268.

(25) Qian, Q.; Yu, G.; Zhao, Q.; Zhang, X. One-Step Hydrothermal Preparation of Bilayer Films of NiCoLDH/Pt Loaded on Nickel Foam Surface for HER Catalytic Activity. *New J. Chem.* **2023**, *47*, 1040−1044.

(26) Iarchuk, A.; Dutta, A.; Broekmann, P. Novel Ni Foam Catalysts for Sustainable Nitrate to Ammonia Electroreduction. *J. Hazard. Mater.* **2022**, *439*, 129504.

(27) Zhang, L.; Zhou, M.; Wang, A.; Zhang, T. Selective Hydrogenation over Supported Metal Catalysts: from Nanoparticles to Single Atoms. *Chem. Rev.* **2020**, *120* (2), 683−733.

(28) Lu, Z.; Tracy, R. W.; Abrams, M. L.; Nicholls, N. L.; Barger, P. T.; Li, T.; Stair, P. C.; Dameron, A. A.; Nicholas, C. P.; Marshall, C. L. Atomic Layer Deposition Overcoating Improves Catalyst Selectivity and Longevity in Propane Dehydrogenation. *ACS Catal.* **2020**, *10* (23), 13957−13967.

(29) George, C.; Littlewood, P.; Stair, P. C. Understanding Pore Formation in ALD Alumina Overcoats. *ACS Appl. Mater. Interfaces* **2020**, *12* (18), 20331−20343.

(30) Cao, K.; Cai, J.; Liu, X.; Chen, R. Review Article: Catalysts Design and Synthesis via Selective Atomic Layer Deposition. *J. Vac. Sci.* **2018**, *36* (1), 010801.

(31) Lu, J.; Liu, B.; Greeley, J. P.; Feng, Z.; Libera, J. A.; Lei, Y.; Bedzyk, M. J.; Stair, P. C.; Elam, J. W. Porous Alumina Protective Coatings on Palladium Nanoparticles by Self-Poisoned Atomic Layer Deposition. *Chem. Mater.* **2012**, *24* (11), 2047−2055.

(32) Aireddy, D. R.; Yu, H.; Cullen, D. A.; Ding, K. Elucidating the Roles of Amorphous Alumina Overcoat in Palladium-Catalyzed Selective Hydrogenation. *ACS Appl. Mater. Interfaces* **2022**, *14* (21), 24290−24298.

(33) Chen, J.; Lim, B.; Lee, E. P.; Xia, Y. Shape-Controlled Synthesis of Platinum Nanocrystals for Catalytic and Electrocatalytic Applications. *Nano Today* **2009**, *4*, 81−95.

(34) Ye, Q.; Xu, W.; Chen, S.; Wang, Z.; Duan, X.; Liu, H.; Zhang, H.; Sun, L.; Yang, W.; Zhang, C.; Zhou, J. Initial Nucleation Process in the Synthesis of Platinum Nanoparticle from Chloroplatinic Acid. *Nano Today* **2021**, *37*, 101093.

(35) Yao, T.; Liu, S.; Sun, Z.; Li, Y.; He, S.; Cheng, H.; Xie, Y.; Liu, Q.; Jiang, Y.; Wu, Z.; Pan, Z.; Yan, W.; Wei, S. Probing Nucleation Pathways for Morphological Manipulation of Platinum Nanocrystals. *J. Am. Chem. Soc.* **2012**, *134* (22), 9410−9416.

(36) Chen, S.; Yang, Q.; Wang, H.; Zhang, S.; Li, J.; Wang, Y.; Chu, W.; Ye, Q.; Song, L. Initial Reaction Mechanism of Platinum Nanoparticle in Methanol-Water System and the Anomalous Catalytic Effect of Water. *Nano Lett.* **2015**, *15* (9), 5961−5968.

(37) Abdulagatov, A.; Yan, Y.; Cooper, J.; Zhang, Y.; Gibbs, Z.; Cavanagh, A.; Yang, R.; Lee, Y.; George, S. Al_2O_3 and TiO_2 Atomic Layer Deposition on Copper for Water Corrosion Resistance. *ACS Appl. Mater. Interfaces* **2011**, *3* (12), 4593−4601.

(38) Carcia, P. F.; McLean, R. S.; Li, Z. G.; Reilly, M. H.; Marshall, W. J. Permeability and Corrosion in ZrO_2/Al_2O_3 Nanolaminate and Al_2O_3 Thin Films Grown by Atomic Layer Deposition on Polymers. *J. Vac. Sci.* **2012**, *30* (4), 041515.

(39) Correa, G. C.; Bao, B.; Strandwitz, N. C. Chemical Stability of Titania and Alumina Thin Films Formed by Atomic Layer Deposition. *ACS Appl. Mater. Interfaces* **2015**, *7* (27), 14816−14821.

(40) Chen, G.; Zhu, X.; Chen, R.; Liao, Q.; Ye, D.; Zhang, B.; Feng, H.; Liu, J.; Liu, M.; Wang, K. Hierarchical Pd@Ni Catalyst with a Snow-like Nanostructure on Ni Foam for Nitrobenzene Hydrogenation. *Appl. Catal.* **2019**, *575*, 238−245.
(41) Chastain, J.; King, R. C. *Handbook of X-ray Photoelectron Spectroscopy*; Perkin-Elmer Corporation, 1992; Vol. *40*, p 221.
(42) Bolt, P.; Ten Grotenhuis, E.; Geus, J.; Habraken, F. The Interaction of Thin NiO Layers with Single Crystalline α-Al_2O_3 (1120) Substrates. *Surf. Sci.* **1995**, *329* (3), 227−240.
(43) Huang, S.; Zhu, X.; Cheng, B.; Yu, J.; Jiang, C. Flexible Nickel Foam Decorated with Pt/NiO Nanoflakes with Oxygen Vacancies for Enhanced Catalytic Formaldehyde Oxidation at Room Temperature. *Environ. Sci. Nano* **2017**, *4* (11), 2215−2224.
(44) McIntyre, N.; Cook, M. X-ray Photoelectron Studies on Some Oxides and Hydroxides of Cobalt, Nickel, and Copper. *Anal. Chem.* **1975**, *47* (13), 2208−2213.
(45) Liu, P.; Ran, J.; Xia, B.; Xi, S.; Gao, D.; Wang, J. Bifunctional Oxygen Electrocatalyst of Mesoporous Ni/NiO Nanosheets for Flexible Rechargeable Zn-Air Batteries. *Nano-Micro Lett.* **2020**, *12*, 68.
(46) Safeer N. K., M.; Alex, C.; Jana, R.; Datta, A.; John, N. S. Remarkable CO_x Tolerance of Ni^{3+} Active Species in a Ni_2O_3 Catalyst for Sustained Electrochemical Urea Oxidation. *J. Mater. Chem. A* **2022**, *10*, 4209−4221.
(47) Yuan, G.; Wang, L.; Zhang, X.; Wang, Q. Self-Supported Pt Nanoflakes-Doped Amorphous $Ni(OH)_2$ on Ni Foam Composite Electrode for Efficient and Stable Methanol Oxidation. *J. Colloid Interface Sci.* **2019**, *536*, 189−195.
(48) Iatsunskyi, I.; Kempiński, M.; Jancelewicz, M.; Załęski, K.; Jurga, S.; Smyntyna, V. Structural and XPS Characterization of ALD Al_2O_3 Coated Porous Silicon. *Vacuum* **2015**, *113*, 52−58.
(49) Tago, T.; Kataoka, N.; Tanaka, H.; Kinoshita, K.; Kishida, S. XPS Study From a Clean Surface of Al_2O_3 Single Crystals. *Procedia Eng.* **2017**, *216*, 175−181.
(50) Schneider, W.-D.; Laubschat, C. Actinide—Noble-Metal Systems: An X-Ray-Photoelectron-Spectroscopy Study of Thorium-Platinum, Uranium-Platinum, and Uranium-Gold Intermetallics. *Phys. Rev. B* **1981**, *23* (3), 997.
(51) Ma, Y.; Chi, B.; Liu, W.; Cao, L.; Lin, Y.; Zhang, X.; Ye, X.; Wei, S.; Lu, J. Tailoring of the Proximity of Platinum Single Atoms on CeO_2 Using Phosphorus Boosts the Hydrogenation Activity. *ACS Catal.* **2019**, *9* (9), 8404−8412.
(52) Jiang, N.; Zhou, X.; Jiang, Y.-F.; Zhao, Z.-W.; Ma, L.-B.; Shen, C.-C.; Liu, Y.-N.; Yuan, C.-Z.; Sahar, S.; Xu, A.-W. Oxygen Deficient Pr_6O_{11} Nanorod Supported Palladium Nanoparticles: Highly Active Nanocatalysts for Styrene and 4-nitrophenol Hydrogenation Reactions. *RSC Adv.* **2018**, *8* (31), 17504−17510.
(53) Liu, P.; Zhao, Y.; Qin, R.; Mo, S.; Chen, G.; Gu, L.; Chevrier, D. M.; Zhang, P.; Guo, Q.; Zang, D.; et al. Photochemical Route for Synthesizing Atomically Dispersed Palladium Catalysts. *Science* **2016**, *352* (6287), 797−800.
(54) Lyu, J.; Wang, J.; Lu, C.; Ma, L.; Zhang, Q.; He, X.; Li, X. Size-Dependent Halogenated Nitrobenzene Hydrogenation Selectivity of Pd Nanoparticles. *J. Phys. Chem. C* **2014**, *118*, 2594−2601.
(55) Hu, M.; Jin, L.; Dang, Y.; Suib, S. L.; He, J.; Liu, B. Supported Pt Nanoparticles on Mesoporous Titania for Selective Hydrogenation of Phenylacetylene. *Front. Chem.* **2020**, *8*, 581512.
(56) Wang, Z.; Garg, A.; Wang, L.; He, H.; Dasgupta, A.; Zanchet, D.; Janik, M. J.; Rioux, R. M.; Román-Leshkov, Y. Enhancement of Alkyne Semi-Hydrogenation Selectivity by Electronic Modification of Platinum. *ACS Catal.* **2020**, *10*, 6763−6770.
(57) Geng, Y.; Chen, C.; Gao, Z.; Feng, X.; Liu, W.; Li, Y.; Jin, T.; Shi, Y.; Zhang, W.; Bao, M. Unsupported Nanoporous Platinum-Iron Bimetallic Catalyst for the Chemoselective Hydrogenation of Halonitrobenzenes to Haloanilines. *ACS Appl. Mater. Interfaces* **2021**, *13*, 23655−23661.
(58) Deng, X.; Wang, J.; Guan, N.; Li, L. Catalysts and Mechanisms for the Selective Heterogeneous Hydrogenation of Carbon-Carbon Triple Bonds. *Cell Rep. Phys. Sci.* **2022**, *3* (9), 101017.
(59) Delgado, J. A.; Benkirane, O.; Claver, C.; Curulla-Ferré, D.; Godard, C. Advances in the Preparation of Highly Selective Nanocatalysts for the Semi-Hydrogenation of Alkynes using Colloidal Approaches. *Dalton Trans.* **2017**, *46*, 12381−12403.

https://doi.org/10.1021/acsami.3c08545
ACS Appl. Mater. Interfaces 2023, 15, 43756−43766